Maximum Possible Cooling Rate in Ultrafast Chip Nanocalorimetry: Fundamental Limitations Due to Thermal Resistance at the Membrane/Gas Interface

Alexander A. Minakov [1] and Christoph Schick [2,3,*]

1 Prokhorov General Physics Institute of the Russian Academy of Sciences, Vavilov Str. 38, 119991 Moscow, Russia; minakov@nsc.gpi.ru
2 Centre CALOR, Institute of Physics and Competence, University of Rostock, 18051 Rostock, Germany
3 Alexander Butlerov Institute of Chemistry, Kazan Federal University, Kremlyovskaya Str. 18, 420008 Kazan, Russia
* Correspondence: christoph.schick@uni-rostock.de

Abstract: Ultrafast chip nanocalorimetry opens up remarkable possibilities in materials science by allowing samples to be cooled and heated at extremely high rates. Due to heat transfer limitations, controlled ultrafast cooling and heating can only be achieved for tiny samples in calorimeters with a micron-thick membrane. Even if ultrafast heating can be controlled under quasi-adiabatic conditions, ultrafast controlled cooling can be performed if the calorimetric cell is located in a heat-conducting gas. It was found that the maximum possible cooling rate increases as $1/r_0$ with decreasing radius r_0 of the hot zone of the membrane. The possibility of increasing the maximum cooling rate with decreasing r_0 was successfully implemented in many experiments. In this regard, it is interesting to answer the question: what is the maximum possible cooling rate in such experiments if r_0 tends to zero? Indeed, on submicron scales, the mean free path of gas molecules l_{mfp} becomes comparable to r_0, and the temperature jump that exists at the membrane/gas interface becomes significant. Considering the limitation associated with thermal resistance at the membrane/gas interface and considering the transfer of heat through the membrane, we show that the controlled cooling rate can reach billions of K/s, up to 10^{10} K/s.

Keywords: chip-nanocalorimetry; ultrafast nanocalorimetry; interfacial thermal resistance

1. Introduction

Ultrafast membrane-based nanocalorimetry opens up exciting opportunities for materials science [1–15]. This calorimetry makes it possible to measure the size-dependent properties of nanosized samples [1,5,9] and films as thin as about 0.1 nm [2,3], as well as measure the melting and synthesis characteristics of a single-layer lamella [7,8], and directly measure the desorption of polymer chains [12]. The ultrafast calorimetry method is described in detail in [10]. A review of microchip-based nanocalorimeters is presented in [11]. It is very important that ultrafast calorimetry allows nano- and microsamples to be heated or quenched at extremely high, controlled rates, creating non-equilibrium states under well-defined conditions, and to study the kinetics of phase transitions on a sub-millisecond time scale. A review of such experiments is presented in [14]. For example, crystallization and recrystallization kinetics [15–20], as well as interfacial thermal conductance [21,22], can be measured in ultrafast membrane nanocalorimeters during rapid melting and crystallization. It was shown that calorimetric measurements with controlled cooling and heating rates up to 10^8 K/s are possible using membrane sensors; in the experiment, an uncontrolled cooling rate of about 10^8 K/s was achieved [23]. However, the fundamental limitations on controlled cooling rates need to be investigated. Indeed, even if ultrafast heating can be controlled in a nanocalorimeter under quasi-adiabatic conditions, ultrafast cooling can only be performed under non-adiabatic conditions [23–26]. In fact, the

central hot zone of the membrane is used as a calorimetric cell. The heat transfer between the hot zone and the environment determines the maximum cooling rate achievable in an experiment. It was found that uniform ultrafast controlled cooling can be accomplished for nanogram samples if the measuring calorimetric cell is placed in heat-conducting nitrogen gas or helium gas [23–26]. For several sensors of different size and geometry, it was shown that the maximum possible controlled cooling rate is proportional to the ratio λ/r_0, where λ is the thermal conductivity of the surrounding gas and r_0 is the radius of the central hot zone of the membrane [23–26]. The possibility of increasing the maximum cooling rate with decreasing r_0 has been successfully used in many experiments [10–26]. The goal of this article is to answer the question: what is the maximum possible cooling rate in such experiments if r_0 tends to zero? Indeed, on submicron scales, the mean free path of gas molecules l_{mfp} becomes comparable to r_0. In fact, there is a jump in temperature ΔT_C at the membrane/gas contact. The temperature jump ΔT_C increases with the increase of the temperature gradient in the gas near the membrane hot zone; this temperature gradient is about $(T - T_t)/r_0$, where T is the temperature of the hot zone, T_t is the temperature of the thermostat. Thus, for r_0 on a submicron scale, a comprehensive analysis of the thermal processes occurring in the calorimetric sensor located in a heat-conducting gas is required.

In the first part of the paper, we consider the thermal resistance at the membrane/gas interface and obtain the fundamental limitation on the maximum possible cooling rate in a membrane-based calorimeter with the calorimetric cell located in a heat-conducting gas. In the second part of the paper, the effect of the heat transfer from the central hot zone of the membrane to the periphery of the membrane is considered. Finally, it is shown that the controlled cooling rate in membrane calorimeters can reach up to ten billion K/s in helium gas.

2. Membrane-Based Ultrafast Nanocalorimeter

The considered membrane-based calorimeter consists of an amorphous silicon nitride membrane with a thin-film resistive heater and a thermocouple located in the center of the membrane, see Figure 1. The central hot zone of the membrane is used as the calorimetric cell. The sample to be measured is placed in the center of this zone, next to the measuring hot junction of the thermocouple, see Figure 1. The thermocouple, heater, and electrical leaders are formed by p- and n-type polysilicon tracks with suitable thermoelectric properties and resistivity. For the protection and electrical insulation, the measuring circuit is covered with a submicron amorphous silicon nitride layer so that the total membrane thickness d_m is about 1 μm. The membrane is attached to a silicon frame at a distance of $b_0 = 350$ μm from the center of the membrane. The frame is mounted on a standard TO-5 housing. The calorimetric cell is located in a thermostat with controlled temperature T_t and gas pressure p.
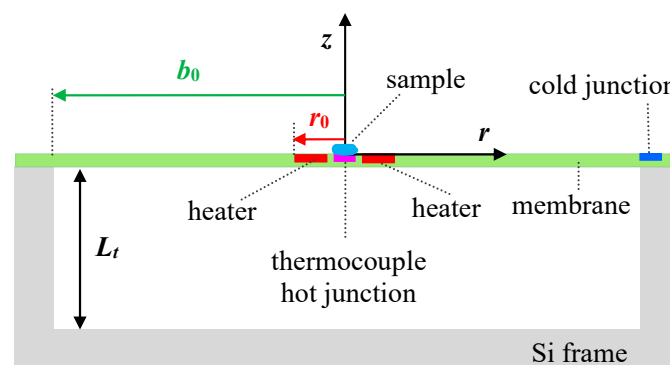

Figure 1. Schematic sectional view of a membrane-based nanocalorimeter, not to scale.

The heat generated by the heater in the hot zone of the membrane is transferred to the surrounding gas and membrane. Consider the transfer of heat to the gas. Let α

denote the coefficient of heat transfer from the membrane surface to the surrounding gas. This coefficient, measured in W/m^2K, describes the heat loss from the central hot zone of the membrane to the gas. The heat losses are mainly associated with the thermal conductivity λ of the surrounding gas [23–26]. This heat loss is proportional to $\frac{\lambda(T-T_t)}{L}$, where L is the characteristic length of the problem. Since r_0 is small with respect to the distance L_t from the hot zone to the thermostat, the heat loss is proportional to $\frac{\lambda(T-T_t)}{r_0}$. In fact, the hot zone can be considered as a spherical (point) heat source embedded in the gas. Consequently, $\alpha = \lambda/r_0$ with good accuracy for a radius r_0 of tens of microns or less [23–26]. The convective and radiative contributions to the heat losses are negligible for such a small r_0, see Appendix A. Thus, the cooling rate R of the hot zone of the membrane depends on the heat transfer parameter $\alpha = \lambda/r_0$ at $L_t \gg r_0 \gg l_{mfp}$.

Typically, nitrogen gas or helium gas is used to cool the membrane [10–26]. In differential scanning calorimetry, the calorimetric cell loaded with the sample and the reference unloaded cell are maintained at the same temperature $T(t)$ in the central hot zone; this temperature is controlled at the desired scanning rate $R(t)$. The difference in input power required to match the temperature of the loaded cell to the temperature of the reference cell is equal to the power $P_S(t)$ absorbed or released from the sample being measured [27]. This study aims to estimate the maximum possible controlled cooling rate R_{max} for membrane calorimeters. Thus, we estimate R_{max} for an unloaded cell, considering the limiting case when the heat capacity of the sample is negligible.

3. Interfacial Thermal Resistance at the Membrane/Gas Interface

Let us consider the change in the gas temperature near the hot zone of the membrane at distances comparable to l_{mfp}. Note that for distances of the order of l_{mfp}, it is necessary to clarify the concept of the gas temperature. Temperature is commonly defined as the average local energy of gas molecules, assuming that the distribution function is the same as for large volumes [28]. Consider the temperature jump ΔT_C at the membrane/gas contact. This jump in temperature means that there is a contact thermal resistance at the interface between the gas and the calorimeter membrane. In this case, the so-called temperature jump distance δ can be introduced [29,30]. In fact, the effect of the temperature jump increases the length of the heat transfer path through the gas by an amount of δ, which is of the order of l_{mfp}. Usually, the boundary condition that takes into account the temperature jump at the membrane/gas interface is represented by Equation (1) [29,30]:

$$T_K - T_m = \delta \frac{\partial T}{\partial z},$$
(1)

where T_m is the temperature of the membrane, and T_K is the gas temperature extrapolated to the membrane, as if the temperature gradient in the gas $\frac{\partial T}{\partial z}$ was not distorted due to the temperature jump at the interface. The temperature jump distance δ depends on the following gas parameters: mean free path l_{mfp}, heat capacity ratio γ, kinematic viscosity ν, and thermal diffusivity $D = \lambda/\rho c_p$, where ρ and c_p are the density and specific heat capacity at constant pressure, respectively. The temperature jump distance δ can be represented by Equation (2) [29,30]:

$$\delta = \left(\frac{2-\sigma}{\sigma}\right)\left(\frac{2\gamma}{1+\gamma}\right)\left(\frac{\lambda}{\nu\rho c_p}\right)l_{mfp},$$
(2)

where σ is the thermal accommodation coefficient in the boundary condition, see Equation (3).

$$T_r = \sigma T_m + T_i(1-\sigma),$$
(3)

where T_i and T_r are the temperatures of the incident and reflected gas molecules; T_m is the membrane temperature [29,30]. In fact, σ denotes the fraction of molecules that are diffusely reflected from the membrane at the temperature T_m. The remaining fraction of molecules

is reflected specularly, which means that their velocity components, perpendicular to the membrane surface, only change sign. Thus, it follows from Equation (3) that σ can be represented as:

$$\sigma = (T_r - T_i)/(T_m - T_i). \tag{4}$$

Equation (4) reveals the physical meaning of the thermal accommodation coefficient σ. The parameter σ depends on the gas molecules and the solid surface with which the gas molecules interact. This parameter becomes close to 1 for a blackened surface [30]. σ is relatively small for light gas molecules. For example, for helium gas and bright platinum σ is about 0.5, and 0.9 for blackened platinum [30]. However, for CO_2 gas, σ is about 1 for various solids [30].

Let us consider the thermal contact conductance G_C at the membrane/gas interface. By definition, the thermal contact conductance G_C is equal to the ratio $q_C/\Delta T_C$, where q_C is the heat flux through the interface [30]. q_C is equal to the product of λ and the temperature gradient in the gas near the interface. ΔT_C is equal to the product of δ and the temperature gradient in the gas near the interface. Thus, the thermal contact conductance G_C is:

$$G_C = \lambda/\delta. \tag{5}$$

Kennard calculated the energy flux $G_{max}(T - T_t)$ from a unit area of a solid in a gas at a constant pressure p, which is the maximum possible heat flux at the solid/gas interface [29,31].

$$G_{max} = (f+1)k_B \frac{\sigma}{(2-\sigma)} \frac{p}{\sqrt{2\pi m k_B T}}, \tag{6}$$

where m and f are the mass and number of degrees of freedom of the gas molecule, respectively. $k_B = 1.38 \cdot 10^{-23}$ J/K is Boltzmann constant [30]. In fact, G_{max} is equal to the thermal contact conductance $G_C = \lambda/\delta$. Indeed, from Equations (2), (5) and (6) we obtain the equality $G_C = G_{max}$ taking into account the equation for the mean free pass $l_{mfp} = v\sqrt{\pi m/2k_B T}$ [32].

Thus, R_{max} for an unloaded cell can be estimated as

$$R_{max} = \frac{2G_{max}(T - T_t)}{\rho_m c_m d_m}, \tag{7}$$

where $d_m = 1$ μm is the membrane thickness and $\rho_m c_m = 2.3 \cdot 10^6$ J/m^{3}K is the volumetric heat capacity of the membrane at the density $\rho_m = 3.2$ g/cm^3 and the specific heat capacity $c_m = 0.71$ J/gK [33]. Suppose $T - T_t = 500$ K, $\sigma = 1$ for a blackened membrane surface, and $r_{min} = \delta$. Then the rate R_{max} can be estimated for several gases, see Table 1. A similar Table 2 is represented for σ corresponding to a bright surface. Data on λ, v, and l_{mfp} for gases are available in [33] and are collected in Tables 1–3. The temperature jump distance δ is calculated using Equation (2). The results of measurements of the thermal accommodation parameter of various gasses on several material are summarized in [30]. A significant scatter of these results shows that uncontrolled defects of the material surface also affect the parameter σ [30]. Since our goal is not to accurately calculate the cooling rate, but to estimate the maximum possible rate, we use the available data for bright and blackened surfaces. In fact, σ depends not so much on the material but significantly on the quality of the surface, therefore in Table 2 we use the data available for some bright solid surfaces and several gases [30].

Table 1. Thermal and contact parameters of gases for a blackened membrane at 300 K and 10^5 Pa.

Gas	Number of Degrees of Freedom of Gas Molecules f Dimensionless	Mean Free Path of Gas Molecules l_{mfp} μm	Temperature Jump Distance δ μm	Thermal Conductivity λ W/m·K	Maximum Possible Parameter $\alpha = \frac{\lambda}{r_{min}}$ MW/m^{2}K	Maximum Interfacial Thermal Conductance G_{max} MW/m^{2}K	Maximum Cooling Rate R_{max} K/s
H$_2$	5	0.126	0.21	0.192	0.90	0.90	$3.9 \cdot 10^8$
He	3	0.200	0.38	0.156	0.41	0.42	$1.8 \cdot 10^8$
N$_2$	5	0.068	0.11	0.026	0.24	0.24	$1.04 \cdot 10^8$
CO$_2$	6	0.045	0.07	0.017	0.22	0.22	$0.96 \cdot 10^8$

Table 2. Thermal and contact parameters of gases for a bright membrane at 300 K and 10^5 Pa.

Gas	Thermal Accom-Modation Coefficient σ Dimensionless	Mean Free Path of Gas Molecules l_{mfp} μm	Temperature Jump Distance δ μm	Thermal Conductivity λ W/m·K	Maximum Possible Parameter $\alpha = \frac{\lambda}{r_{min}}$ MW/m^{2}K	Maximum Interfacial Thermal Conductance G_{max} MW/m^{2}K	Maximum Cooling Rate R_{max} K/s
H$_2$	0.7	0.126	0.40	0.192	0.48	0.48	$2.1 \cdot 10^8$
H$_2$	0.5	0.126	0.64	0.192	0.30	0.30	$1.3 \cdot 10^8$
N$_2$	0.95	0.068	0.12	0.026	0.21	0.22	$0.9 \cdot 10^8$
He	0.5	0.200	1.13	0.156	0.14	0.14	$0.6 \cdot 10^8$

Table 3. Thermal parameters of gases at 300 K and 10^5 Pa.

Gas	Mean Free Path l_{mfp} μm	Thermal Diffusivity D m^2/s	Thermal Diffusion Time $\tau_D = r_0^2/D$ s	Average Velocity of Gas Molecules $V_m = \sqrt{8k_BT/\pi m}$ km/s	Average Time between Collisions $\tau_m = l_{mfp}/V_m$ s
H$_2$	0.126	$1.6 \cdot 10^{-4}$	$6.2 \cdot 10^{-9}$	1.78	$0.7 \cdot 10^{-10}$
He	0.200	$1.9 \cdot 10^{-4}$	$5.3 \cdot 10^{-9}$	1.26	$1.6 \cdot 10^{-10}$
N$_2$	0.068	$2.2 \cdot 10^{-5}$	$45 \cdot 10^{-9}$	0.476	$1.4 \cdot 10^{-10}$

Figure 2 shows the dependence of the rate R on r_0 for different gases, obtained by Equation (8).

$$R = \frac{2\lambda(T - T_t)/r_0}{\rho_m c_m d_m}. \tag{8}$$

R increases as $1/r_0$ up to the maximum possible rate corresponding to the maximum possible heat flux $G_{max}(T - T_t)$, see Equation (6). For the estimation of R_{max}, the thermal parameters of the gas and membrane are considered independent of temperature. In fact, the heat capacity of the membrane changes insignificantly at temperatures above 300 K [33]. The increase in gas thermal conductivity λ with increasing temperature [33] is compensated by an increase of the temperature jump distance δ. Thus, we get approximately the same R_{max} (with an accuracy of about 30%) for thermal parameters corresponding to 600 K; these parameters are available in [33]. The uncertainty in σ (which depends on the surface quality) is more significant. Thus, we obtain an estimate of the maximum possible interfacial thermal conductance (G_{max}) and the minimum radius ($r_{min} \geq \delta$) of the hot zone of the membrane.
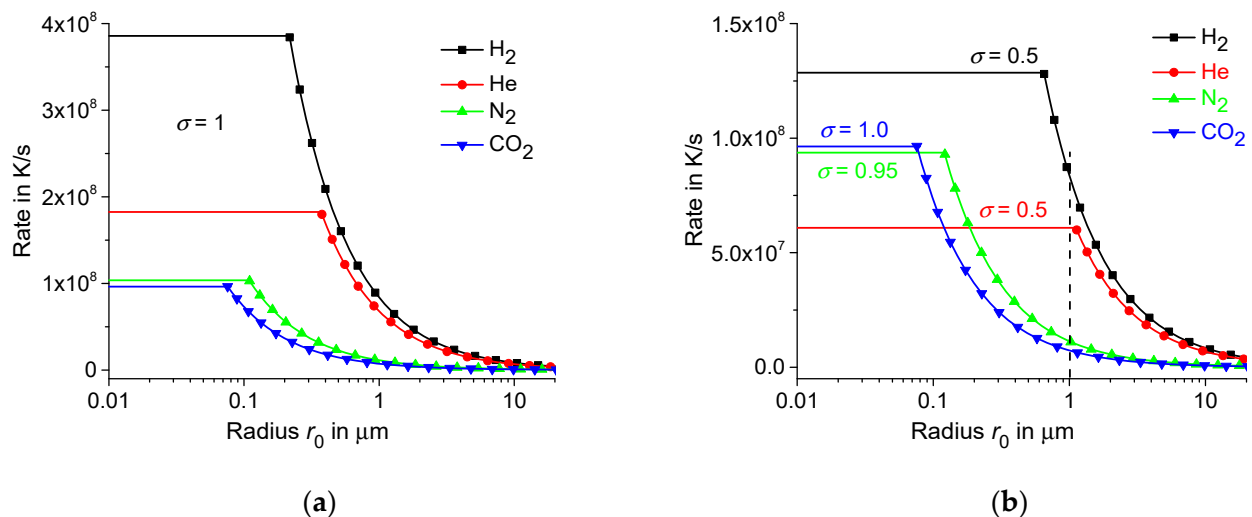

Figure 2. Possible cooling rate R vs. the radius r_0 of the hot zone for blackened (**a**) and bright (**b**) membrane surfaces for different gases.

In fact, it makes no sense to reduce the radius r_0 to less than 1 μm, at least for the most heat-conducting hydrogen and helium gases, see Table 2 and Figure 2b. Thus, a cooling rate 10^8 K/s is possible at r_0 of about 1 μm. However, the maximum possible cooling rate R_{max} is even higher due to the additional heat transfer from the hot zone of the membrane to the periphery of the membrane. Thus, it is necessary to consider the problem of heat transfer for the entire membrane-gas system. Next, we estimate the rate R_{max} for helium gas as one of the most suitable and heat-conducting gases at $r_0 = 1$ μm and different thermal conductivity λ_m of the membrane.

4. Maximum Possible Controlled Cooling Rate in the Membrane-Gas System

Heat in gases is transferred by molecules moving at a speed sufficient to achieve high cooling rates. In fact, a cooling rate of about 10^8 K/s was achieved in the experiment [23]. The diffusion Fourier heat equation for gasses is a good approximation on a time scale that is much larger than the average time between collisions of gas molecules [28,34]. Denoted by $\tau_m = l_{mfp}/V_m$ the average time between collisions of gas molecules, where $V_m = \sqrt{8k_BT/\pi m}$ is the average velocity of gas molecules [32,33]. In fact, $\tau_m = 0.07$ ns, 0.16 ns, and 0.14 ns for hydrogen, helium, and nitrogen gases at $V_m = 1.78$ km/s, 1.26 km/s, and 0.476 km/s, respectively (see Table 3). The thermal perturbation in the gas around the

heated region of radius r_0 relaxes during the thermal diffusion time $\tau_D = r_0^2/D$. In fact, $\tau_D = 6.2$ ns, 5.3 ns, and 45 ns at $D = 1.6 \cdot 10^{-4}$ m^2/s, $1.9 \cdot 10^{-4}$ m^2/s, and $2.2 \cdot 10^{-5}$ m^2/s for hydrogen, helium, and nitrogen gases, respectively, at $r_0 = 1$ μm. The thermal parameters of the gases are available in [33] and collected in Table 3. Thus, τ_D is much longer than the average time between collisions of gas molecules, $\tau_D \gg \tau_m$, and about 10^2 collisions per molecule occurs during τ_D. In this case, the diffusion Fourier heat equation can be used [28,34]. However, the limited rate of relaxation of thermal perturbations in the gas imposes the following limitation on the cooling rate: $R < \Delta T/\tau_D$, where ΔT is the interval of the temperature scanning. Assume $\Delta T = 1000$ K, then the cooling rate R is limited to about $1.6 \cdot 10^{11}$ K/s, $2 \cdot 10^{11}$ K/s, and $2 \cdot 10^{10}$ K/s for hydrogen, helium, and nitrogen gases, respectively. This limitation is not the most significant. The main restriction is associated with thermal relaxation of the membrane–gas system; this relaxation depends on the heat loss from the membrane, which mainly depends on the thermal conductivity of the gas λ.

Let us consider the temperature distribution $T(t, r)$ in the lateral direction of the membrane for a ring-shaped heater. The temperature difference in the z direction is insignificant, since λ is much less than the membrane thermal conductivity λ_m. Note that the temperature gradients near the central hot zone in the gas and membrane are approximately the same and equal to $(T - T_t)/r_0$. Therefore, $\partial T/\partial z$ is about $(\lambda/\lambda_m)\partial T/\partial r$, as follows from the boundary condition for the heat flux at the membrane/gas interface. Thus, gradients along the z direction in the membrane can be neglected at $\lambda \ll \lambda_m$. In addition, the temperature distribution $T(t, r)$ tends to zero at a distance of the order of r_0, see below. Thus, the shape of the membrane at the periphery does not matter at $r \gg r_0$. Therefore, we consider a boundary value problem with a homogeneous boundary condition $T(t, b_0) = 0$, where b_0 is the distance from the center of the membrane to the silicon frame, the temperature of which is equal to the temperature of the thermostat, and the temperature $T(t, r)$ is measured from T_t. Thus, for the membrane–gas system, we have an equation for $T(t, r)$ in cylindrical coordinates, see Equation (9). The second term $(-T/\tau)$ on the right-hand side of Equation (9) describes the heat loss from the membrane to the gas.

$$\frac{\partial T}{\partial t} = D_m \left(\frac{\partial^2 T}{\partial r^2} + \frac{1}{r}\frac{\partial T}{\partial r} \right) - \frac{T}{\tau} + \Phi(t, r), \tag{9}$$

where $D_m = \lambda_m/\rho_m c_m$ is the thermal diffusivity of the membrane, $\tau = \rho_m c_m d_m/\alpha$, $\alpha = \lambda/r_0$, $\Phi(t, r) = HF(t, r)/\rho_m c_m d_m$, and $HF(t, r)$ is the surface density of the heat flux generated by the heater [35]. The solution to the problem can be represented as a series expansion:

$$T(t, r) = \sum_{n=1}^{N} J_0(\mu_n r/b_0)\psi_n(t), \tag{10}$$

where $J_0(\mu_n r/b_0)$ are the orthogonal Bessel functions of the first kind and of zero order, $\{\mu_n\}$ is a monotonously increasing sequence of positive roots of the equation $J_0(\mu_n) = 0$ for $n = 1, 2, 3 \ldots$, and N is the number of terms in the series expansion sufficient to achieve the required accuracy. Note that the structure within the hot zone can be accurately calculated if the number N is large compared to b_0/b_1, where b_1 is the thickness of the thinnest heater structure. Good accuracy can be achieved with $N \geq 1000$ for $b_1 = 1/3$ μm and $b_0 = 350$ μm. Further calculations are performed at $N = 2000$. In fact, the difference in the results for $N = 1000$ and 2000 was insignificant.

The functions $\psi_n(t)$ can be obtained from the Fourier components of Equation (9).

$$\partial \psi_n(t)/\partial t + \left(\tau^{-1} + \tau_n^{-1} \right)\psi_n(t) = B_n(t), \tag{11}$$

where $\tau_n = 1/D_m(\mu_n/b_0)^2$ and

$$B_n(t) = \frac{2}{b_0^2 J_1(\mu_n)^2} \int_0^{b_0} J_0(\mu_n r/b_0)\Phi(t, r)r dr. \tag{12}$$

Consider the solution $T(t,r)$ for a ring heater. Suppose $\Phi(t,r) = q(t)F(r)$, where $F(r) = 1$ in the ring $r \in (r_1, r_0)$ and $F(r) = 0$ outside this ring. Thus,

$$B_n(t) = \frac{q(t)}{\rho_m c_m d_m} \frac{2r_0 J_1(\mu_n r_0/b_0) - 2r_1 J_1(\mu_n r_1/b_0)}{\mu_n b_0 J_1(\mu_n)^2}, \tag{13}$$

where $q(t) = P(t)/\pi(r_0^2 - r_1^2)$ and $P(t)$ is the heater power. Therefore, with a zero initial condition $T(t,r) = 0$ at $t \le 0$, we obtain a solution to Equation (11):

$$\psi_n(t) = \int_0^t B_n(t') \exp\left(-\left(\tau^{-1} + \tau_n^{-1}\right)(t - t')\right) dt'. \tag{14}$$

For model calculations, in order to obtain approximately constant heating and cooling rates, we take the power $P(t)$ increasing as $(t/t_0)^{\beta_1}$ during heating and decreasing as $1 - ((t - t_0)/t_1)^{\beta_2}$ during cooling, where t_0 and t_1 are the duration of temperature scanning during heating and cooling, respectively, β_1 and β_2 are positive parameters less than 1. Thus, we obtain the temperature distribution $T(t,r)$ calculated at $R = 10^8$ K/s and $3 \cdot 10^8$ K/s, see Figure 3. The calculations were carried out for helium gas with $\lambda = 0.156$ W/m·K at $r_0 = 1$ μm, $r_1 = 2r_0/3$, $d_m = 1$ μm, $\lambda_m = 3$W/m·K, $D_m = 1.3 \cdot 10^{-6}$ m²/s, $\rho_m c_m = 2.3 \cdot 10^6$ J/m³K, and the scanning temperature range $\Delta T = 1000$ K. The temperature profile $T(t_0, r)$ was calculated at the end of heating for $t_0 = 10.8$ μs and 3.65 μs at $R = 10^8$ K/s and $3 \cdot 10^8$ K/s, respectively.
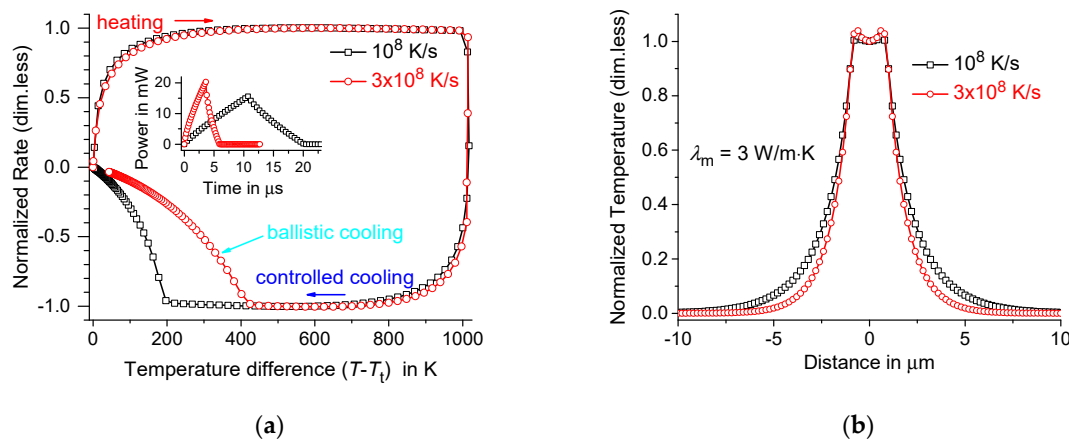

Figure 3. Normalized scanning rate $\partial T/\partial t$ vs. temperature at the center of the membrane for the power $P(t)$ shown in the inset (**a**) and the temperature profile $T(t_0, r)$ (**b**) for $R = 10^8$ K/s and $3 \cdot 10^8$ K/s—black squares and red circles, respectively. The heater acts uniformly in the ring $r \in (r_1, r_0)$ at $r_1 = 2r_0/3$. Thermal conductivity of the membrane $\lambda_m = 3$ W/m·K.

Thus, controlled cooling is possible at $R = 10^8$ K/s and even $3 \cdot 10^8$ K/s. Note that at $R = 3 \cdot 10^8$ K/s, ballistic (uncontrolled) cooling begins at some critical temperature difference $(T_C - T_t)$ of about 400 K. This critical temperature difference $(T_C - T_t)$ increases with increasing R, so that controlled cooling above $5 \cdot 10^8$ K/s is practically impossible, even with a scanning interval as large as $\Delta T = 1000$ K.

However, the controlled cooling rate can be increased by additional heat transfer in a membrane with a higher thermal conductivity λ_m. The thermal conductivity λ_m can be increased by depositing an additional heat-conducting Au layer on the membrane. This idea was successfully demonstrated on a commercially available chip calorimeter with a hot zone radius r_0 of about 5 μm [23]. A rate of about 10^8 K/s was achieved in helium gas for a sensor with an additional heat-conducting Au layer on the membrane [23]. In this article, we estimate the maximum possible cooling rate as r_0 decreases. In fact, for an additional Au layer with a thickness d_{Au} and thermal conductivity $\lambda_{Au} = 317$ W/m·K [33], we obtain a membrane with $\lambda_m = \lambda_{Au}(d_{Au}/d_0) + \lambda_0(d/d_0)$ in the lateral direction of the membrane, where d_0 is the thickness of the silicon nitride layer. Suppose $d_0 = 0.8$ μm and $d_{Au} = 0.4$ μm,

then $d_m = 1.2$ μm, $\lambda_m = 100$ W/m·K, and the average volumetric heat capacity of the membrane is $\rho_m c_m = 2.4 \cdot 10^6$ J/m^{3}K at $\rho_{Au} c_{Au} = 2.5 \cdot 10^6$ J/m^{3}K for Au [33]. In this case, controlled cooling is possible at $R = 10^9$ K/s and even at $6 \cdot 10^9$ K/s, see Figure 4. The calculations were carried out for helium gas with $\lambda = 0.156$ W/m·K at $r_0 = 1$ μm, $r_1 = 2r_0/3$, $d_m = 1.2$ μm, $\lambda_m = 100$ W/m·K, $D_m = 4.2 \cdot 10^{-5}$ m^2/s, $\rho_m c_m = 2.4 \cdot 10^6$ J/m^{3}K, and $\Delta T = 1000$ K. The temperature profile $T(t_0, r)$ was calculated at the end of heating for $t_0 = 1.03$ μs and 0.177 μs at $R = 10^9$ K/s and $6 \cdot 10^9$ K/s, respectively.
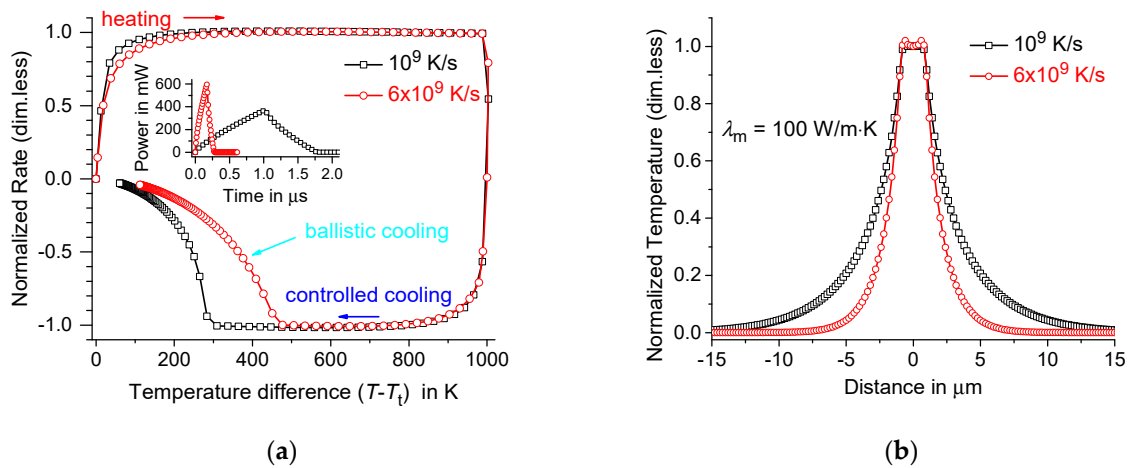

(**a**)   (**b**)

Figure 4. Normalized scanning rate $\partial T / \partial t$ vs. temperature in the center of the membrane for the power $P(t)$ shown in the inset (**a**) and the temperature profile $T(t_0, r)$ (**b**) for $R = 10^9$ K/s and $6 \cdot 10^9$ K/s—black squares and red circles, respectively. The heater acts uniformly in the ring $r \in (r_1, r_0)$ at $r_1 = 2r_0/3$. Thermal conductivity of the membrane $\lambda_m = 100$ W/m·K.

The maximum possible rate of controlled cooling can be even higher if the heater is uniformly distributed over the entire hot zone for $r \in (0, r_0)$. However, in this case, the temperature profile in the middle of the hot zone is not as flat as in the case of the ring heater, see Figures 4 and 5. Controlled cooling is possible at $R = 10^9$ K/s, $6 \cdot 10^9$ K/s, and even 10^{10} K/s, see Figure 5. The calculations were carried out for helium gas with $\lambda = 0.156$ W/m·K at $r_0 = 1$ μm, $d_m = 1.2$ μm, $\lambda_m = 100$ W/m·K, $D_m = 4.2 \cdot 10^{-5}$ m^2/s, $\rho_m c_m = 2.4 \cdot 10^6$ J/m^{3}K, and $\Delta T = 1000$ K. The temperature profile $T(t_0, r)$ was calculated at the end of heating for $t_0 = 1.03$ μs, 0.175 μs, and 0.105 μs at $R = 10^9$ K/s, $6 \cdot 10^9$ K/s, and 10^{10} K/s, respectively.
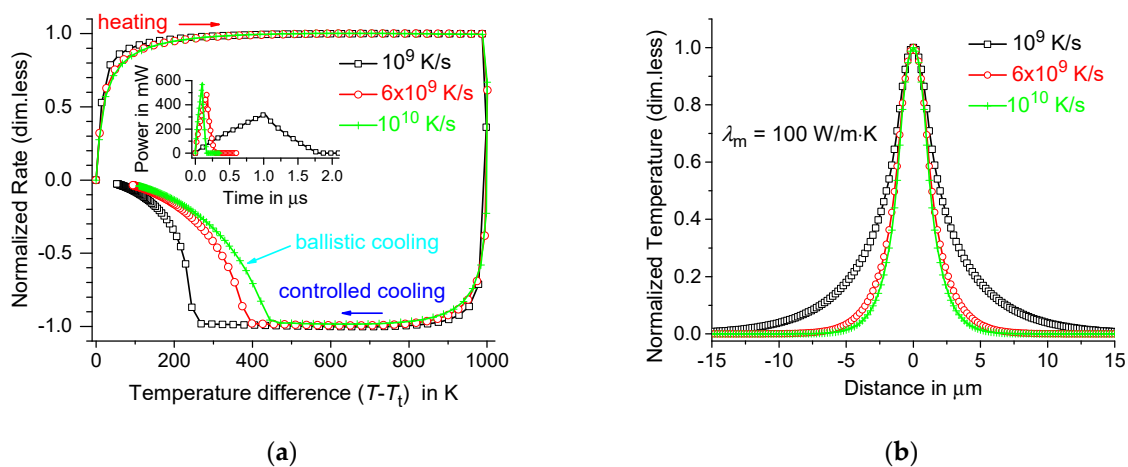

(**a**)   (**b**)

Figure 5. Normalized scanning rate $\partial T / \partial t$ vs. temperature in the center of the membrane for the power $P(t)$ shown in the inset (**a**) and the temperature profile $T(t_0, r)$ (**b**) for $R = 10^9$ K/s, $6 \cdot 10^9$ K/s, and 10^{10} K/s—black squares, red circles, and green crosses, respectively. The heater acts uniformly in the disk $r \in (0, r_0)$. Thermal conductivity of the membrane $\lambda_m = 100$ W/m·K.

5. Conclusions

The controlled maximum possible cooling rate is limited due to the fundamental heat transfer limitation associated with the thermal resistance at the membrane/gas interface. Heat losses from the membrane due to thermal conductivity λ of the surrounding gas are proportional to the heat transfer parameter $\alpha = \lambda/r_0$, which increases with decreasing of the radius of the membrane hot zone r_0 if $L_t \gg r_0 \gg l_{mfp}$. However, the possibility of decreasing the radius r_0 is limited by the temperature jump distance δ. Thus, it makes no sense to reduce the radius r_0 to less than 1 μm, at least for the most heat-conducting gases hydrogen and helium. In fact, this limitation is associated with the maximum possible value of the heat flux $G_{max}(T - T_t)$ at the membrane/gas interface, where the maximum interfacial thermal conductance G_{max} is about 0.9 MW/m^{2}K and 0.42 MW/m^{2}K for a blackened membrane ($\sigma = 1$) and the most heat-conducting gases hydrogen and helium, respectively. Thus, for a free blackened membrane, the maximum cooling rate $2G_{max}(T - T_t)/(\rho_m c_m d_m)$ is about $3.9 \cdot 10^8$ K/s and $1.8 \cdot 10^8$ K/s at $(T - T_t) = 500$ K for hydrogen and helium gases, respectively. Solving the heat transfer problem for the complete membrane-gas system, we find that the maximum possible controlled cooling rate is about $3 \cdot 10^8$ K/s for a silicon nitride membrane with a thickness of 1 μm in helium gas. However, the controlled cooling rate can be increased using the combined membrane with a higher thermal conductivity. Thus, a controlled cooling rate of the order of billions of K/s (up to 10^{10} K/s) is possible for helium gas, $r_0 = 1$ μm, and $(T - T_t) = 1000$ K.

Institutional Review Board Statement: Not applicable.

Informed Consent Statement: Not applicable.

Data Availability Statement: The datasets generated during and/or analyzed during the current study are available from the corresponding author on reasonable request.

Conflicts of Interest: The authors declare no conflict of interest.

Nomenclature

Latin Symbols

b_0	distance from the center to the periphery of the membrane (m)
c_p, c_m	specific heat of gas and membrane at constant p (J/kgK)
D, D_m	thermal diffusivity of gas and membrane (m^2/s)
d_m	membrane thickness (m)
f	number of degrees of freedom of a gas molecule (dimensionless)
g	acceleration of gravity (m/s^2)
G_C	thermal contact conductance (W/m^{2}K)
G_{max}	membrane/gas maximum thermal conductance (W/m^{2}K)
Gr	Grashof number (dimensionless)
k_B	Boltzmann constant (J/K)
l_{mfp}	mean-free-path (m)
L_t	distance from the membrane hot zone to the thermostat (m)
m	mass of a gas molecule (kg)
Nu	Nusselt number (dimensionless)
Pr	Prandtl number (dimensionless)
p	pressure (Pa)
$P(t)$	heater power (W)
q_C	heat flux through thermal contact (W/m^2)
$R(t)$	temperature scan rate (K/s)

R_{max}	maximum possible cooling rate (K/s)
r_0	radius of the hot zone of the membrane (m)
r_{min}	minimum radius of the hot zone (m)
t_0	scan duration on heating (s)
T_t	thermostat temperature (K)
$T_C - T_t$	critical temperature difference of controlled cooling (K)
V_m	average velocity of gas molecules (m/s)

Greek Symbols

α	heat transfer coefficient W/m^{2}K
α_C	convective contribution to the heat transfer coefficient W/m^{2}K
α_r	radiative contribution to the heat transfer coefficient W/m^{2}K
γ	heat capacity ratio (dimensionless)
δ	temperature jump distance (m)
ΔT	scanning temperature range (K)
ΔT_C	temperature jump at the membrane/gas contact (K)
ε	membrane emissivity (dimensionless)
λ, λ_m	thermal conductivity of gas and membrane (W/K · m)
ν	kinematic viscosity of gas (m^2/s)
ρ, ρ_m	density of gas and membrane (kg/m^3)
σ	thermal accommodation coefficient (dimensionless)
σ_r	Stefan-Boltzmann constant (W/m^{2}K^4)
τ	time constant (s)
τ_D	thermal diffusion time (s)
τ_m	average time between collisions (s)
τ_n	time constant of nth component (s)
$\Phi(t,r)$	reduced heat flux (K/s)
$\psi_n(t)$	nth Fourier component (K)

Appendix A. Radiative and Convective Contributions to Membrane Heat Loss

The radiative contribution to the heat transfer coefficient is $\alpha_r = \varepsilon \sigma_t \left(T^4 - T_t^4\right)/(T - T_t)$, where the Stefan-Boltzmann constant $\sigma_r = 5.67 \cdot 10^{-8}$ W/(m^{2}K^4) [33] and the emissivity of the silicon nitride membrane $\varepsilon \leq 0.2$ [36,37]. Therefore, $\alpha_r = 16$ W/(m^{2}K) at $T = 1000$ K and $T_t = 300$ K. Thus, α_r/α is about 0.01% at $\alpha = \lambda/r_0$, which is about $1.56 \cdot 10^5$ W/(m^{2}K) for helium gas $\lambda = 0.156$ W/m·K and $r_0 = 1$ μm. Then α_r is negligible compared to α.

The convective component α_C of the heat losses from the membrane decreases with a decrease in the characteristic length of the problem [21,22,35]. Convective heat losses arise due to the temperature dependence of the gas density in the gravitational field in the presence of temperature gradients. The ratio α_C/α is equal to the Nusselt number $Nu = (Gr)^{1/4} f(Pr)$ [38]. The Prandtl number Pr and $f(Pr)$. for gases are about 1 [33,38]. The Grashof number $Gr = \frac{r_0^3 g}{\nu^2} \frac{(T - T_t)}{T}$ [38], where g is the acceleration due to gravity. Thus, the Nusselt number Nu decreases as $r_0^{3/4}$ with decreasing r_0. In fact, $(Gr)^{1/4}$ is about or less than $\left(r_0^3 g/\nu^2\right)^{0.25} = 5 \cdot 10^{-3}$ at $r_0 = 1$ μm and $\nu = 1.24 \cdot 10^{-4}$ m^2/s [33], that is, $Nu < 0.005$. Convective heat loss only acts on the upper side of the membrane. However, heat losses due to thermal conductivity λ of the surrounding gas act on both sides of the membrane. Thus, the convective contribution to the membrane heat loss $Nu/2\alpha$ is about 0.25% for $r_0 = 1$ μm.

References

1. Lai, S.L.; Guo, J.Y.; Petrova, V.; Ramanath, G.; Allen, L.H. Size-dependent melting properties of small tin particles: Nanocalorimetric measurements. *Phys. Rev. Lett.* **1996**, *77*, 99–102. [CrossRef]
2. Zhang, M.; Efremov, M.Y.; Schiettekatte, F.; Olson, E.A.; Kwan, A.T.; Lai, S.L.; Wisleder, T.; Greene, J.E.; Allen, L.H. Size-dependent melting point depression of nanostructures: Nanocalorimetric measurements. *Phys. Rev. B* **2000**, *62*, 10548–10557. [CrossRef]
3. Efremov, M.Y.; Olson, E.A.; Zhang, M.; Lai, S.L.; Schiettekatte, F.; Zhang, Z.S.; Allen, L.H. Thin-film differential scanning nanocalorimetry: Heat capacity analysis. *Thermochim. Acta* **2004**, *412*, 13–23. [CrossRef]
4. Zhang, M.; Wen, J.G.; Efremov, M.Y.; Olson, E.A.; Zhang, Z.S.; Hu, L.; de la Rama, L.P.; Kummamuru, R.; Kavanagh, K.L.; Ma, Z.; et al. Metastable phase formation in the Au-Si system via ultrafast nanocalorimetry. *J. Appl. Phys.* **2012**, *111*, 093516. [CrossRef]
5. De La Rama, L.P.; Hu, L.; Ye, Z.; Efremov, M.Y.; Allen, L.H. Size effect and odd-even alternation in the melting of single and stacked AgSC n layers: Synthesis and nanocalorimetry measurements. *J. Am. Chem. Soc.* **2013**, *135*, 14286–14298. [CrossRef]
6. Molina-Ruiz, M.; Lopeandía, A.F.; González-Silveira, M.; Anahory, Y.; Guihard, M.; Garcia, G.; Clavaguera-Mora, M.T.; Schiettekatte, F.; Rodríguez-Viejo, J. Formation of Pd2Si on single-crystalline Si (100) at ultrafast heating rates: An in-situ analysis by nanocalorimetry. *Appl. Phys. Lett.* **2013**, *102*, 143111. [CrossRef]
7. Ye, Z.; De La Rama, L.P.; Hu, L.; Efremov, M.Y.; Allen, L.H. Nanocalorimetry study of the evolution of melting characteristics of single layer silver alkanethiolate lamella: Fast heating/cooling and electrical annealing. *Thermochim. Acta* **2015**, *603*, 69–78. [CrossRef]

8.	Ye, Z.; De La Rama, L.P.; Efremov, M.Y.; Zuo, J.M.; Allen, L.H. Approaching the size limit of organometallic layers: Synthesis and characterization of highly ordered silver-thiolate lamellae with ultra-short chain lengths. *Dalton Trans.* **2016**, *45*, 18954–18966. [CrossRef] [PubMed]

9.	Ye, Z.; De La Rama, L.P.; Efremov, M.Y.; Sutrisno, A.; Allen, L.H. Critical Size for Bulk-to-Discrete Transition in 2D Aliphatic Layers: Abrupt Size Effect Observed via Calorimetry and Solid-State 13C NMR. *J. Phys. Chem. C* **2017**, *121*, 13916–13929. [CrossRef]

10.	Schick, C.; Mathot, V. *Fast Scanning Calorimetry*; Springer: Cham, Switzerland, 2016. [CrossRef]

11.	Yi, F.; LaVana, D.A. Nanocalorimetry: Exploring materials faster and smaller. *Appl. Phys. Rev.* **2019**, *6*, 031302. [CrossRef]

12.	Monnier, X.; Napolitano, S.; Cangialosi, D. Direct observation of desorption of a melt of long polymer chains. *Nat. Commun.* **2020**, *11*, 4354. [CrossRef]

13.	Monnier, X.; Marina, S.; Lopez de Pariza, X.; Sardón, H.; Martin, J.; Cangialosi, D. Physical Aging Behavior of a Glassy Polyether. *Polymers* **2021**, *13*, 954. [CrossRef] [PubMed]

14.	Gao, Y.; Zhao, B.; Vlassak, J.J.; Schick, C. Reprint of: Nanocalorimetry: Door opened for in situ material characterization under extreme non-equilibrium conditions. *Prog. Mater. Sci.* **2021**, *120*, 100819. [CrossRef]

15.	Simon, C.; Gao, J.; Mao, Y.; Wilde, G. Fast scanning calorimetric study of nucleation rates and nucleation transitions of Au-Sn alloys. *Scr. Mater.* **2017**, *139*, 13–16. [CrossRef]

16.	Mileva, D.; Wang, J.; Gahleitner, M.; Jariyavidyanont, K.; Androsch, R. New Insights into Crystallization of Heterophasic Isotactic Polypropylene by Fast Scanning Chip Calorimetry. *Polymers* **2020**, *12*, 1683. [CrossRef] [PubMed]

17.	Yang, B.; Peng, Q.; Milkereit, B.; Springer, A.; Liu, D.; Rettenmayr, M.; Schick, C.; Keßler, O. Nucleation behaviour and microstructure of single Al-Si12 powder particles rapidly solidified in a fast scanning calorimeter. *J. Mater. Sci.* **2021**, *56*, 12881–12897. [CrossRef]

18.	Zhang, R.; Du, M.; Zhuravlev, E.; Androsch, R.; Schick, C. Surface crystal nucleation and growth in poly (ε-caprolactone): Atomic force microscopy combined with fast scanning chip calorimetry. *Polymers* **2021**, *13*, 2008. [CrossRef]

19.	Lapuk, S.E.; Mukhametzyanov, T.A.; Schick, C.; Gerasimov, A.V. Crystallization kinetics and glass-forming ability of rapidly crystallizing drugs studied by Fast Scanning Calorimetry. *Int. J. Pharm.* **2021**, *599*, 120427. [CrossRef]

20.	Lee, D.; Zhao, B.; Perim, E.; Zhang, H.; Gong, P.; Gao, Y.; Liue, Y.; Toher, C.; Curtarolo, S.; Schroers, J.; et al. Crystallization behavior upon heating and cooling in Cu50Zr50 metallic glass thin films. *Acta Mater.* **2016**, *121*, 68–77. [CrossRef]

21.	Minakov, A.; Morikawa, J.; Zhuravlev, E.; Ryu, M.; Schick, C. Thermal contact conductance at melting and crystallization of metal micro-droplets. *Mater. Res. Express* **2020**, *7*, 066524. [CrossRef]

22.	Minakov, A.; Morikawa, J.; Ryu, M.; Zhuravlev, E.; Schick, C. Variations of interfacial thermal conductance at melting and crystallization of an indium micro-particle in contact with a solid. *Mater. Des.* **2021**, *201*, 109475. [CrossRef]

23.	Minakov, A.; Morikawa, J.; Zhuravlev, E.; Ryu, M.; van Herwaarden, A.W.; Schick, C. High-speed dynamics of temperature distribution in ultrafast (up to 10^8 K/s) chip-nanocalorimeters, measured by infrared thermography of high resolution. *J. Appl. Phys.* **2019**, *125*, 054501. [CrossRef]

24.	Minakov, A.A.; van Herwaarden, A.W.; Wien, W.; Wurm, A.; Schick, C. Advanced non-adiabatic ultrafast nanocalorimetry and superheating phenomenon in linear polymers. *Thermochim. Acta* **2007**, *461*, 96–106. [CrossRef]

25.	Minakov, A.A.; Schick, C. Ultrafast thermal processing and nanocalorimetry at heating and cooling rates up to 1 MK/s. *Rev. Sci. Instr.* **2007**, *78*, 073902–073910. [CrossRef] [PubMed]

26.	Minakov, A.A.; Schick, C. Dynamics of the temperature distribution in ultra-fast thin-film calorimeter sensors. *Thermochim. Acta* **2015**, *603*, 205–217. [CrossRef]

27.	Zhuravlev, E.; Schick, C. Fast scanning power compensated differential scanning nano-calorimeter: 1. The device. *Thermochim. Acta* **2010**, *505*, 1–13. [CrossRef]

28.	Landau, L.D.; Lifshitz, E.M. *Course of Theoretical Physics 10: Physical Kinetics*, 1st ed.; Pergamon Press: Oxford, UK; Frankfurt, Germany, 1981. [CrossRef]

29.	Kennard, E.H. Kinetic Theory of Gases. In *With an Introduction to Statistical Mechanics*; McGraw-Hill Book Company, Inc.: New York, NY, USA; London, UK, 1938. [CrossRef]

30.	Madhusudana, C.V. *Thermal Contact Conductance. Mechanical Engineering Series*, 2nd ed.; Springer: Cham, Switzerland, 2014.

31.	Liang, Z.; Evans, W.; Keblinski, P. Equilibrium and nonequilibrium molecular dynamics simulations of thermal conductance at solid-gas interfaces. *Phys. Rev. E* **2013**, *87*, 022119. [CrossRef] [PubMed]

32.	Vincenti, W.G.; Kruger, C.H. *Introduction to Physical Gas Dynamics*; Wiley: New York, NY, USA, 1965.

33.	Lide, D.R. *Crc Handbook of Chemistry and Physics*, 90th ed.; CRC Press: Boca Raton, FL, USA, 2010.

34.	Zhang, Z.M. *Nano/Microscale Heat Transfer*, 2nd ed.; Springer International Publishing: Singapore, 2020; ISBN 978-3-030-45039-7. [CrossRef]

35.	Minakov, A.A. Temperature gradients in ultrafast thin-film nanocalorimetry. *Thermochim. Acta* **2019**, *677*, 32–41. [CrossRef]

36.	Jacquot, A.; Chen, G.; Scherrer, H.; Dauscher, A.; Lenoir, B. Improvements of on-membrane method for thin-film thermal conductivity and emissivity measurements. *Sens. Actuators A Phys.* **2005**, *117*, 203–210. [CrossRef]

37.	Van Zwol, P.J.; Vles, D.F.; Voorthuijzen, W.P.; Peter, M.; Vermeulen, H.; Van der Zande, W.J.; Sturm, J.M.; van der Kruijs, R.W.E.; Bijkerk, F. Emissivity of freestanding membranes with thin metal coatings. *J. Appl. Phys.* **2015**, *118*, 213107. [CrossRef]

38.	Landau, L.D.; Lifshitz, E.M. *Course of Theoretical Physics 6: Fluid Mechanics*, 2nd ed.; Butterworth–Heinemann: Oxford, UK, 2000.